Received: 25 April 2019 | Revised: 27 September 2019 | Accepted: 2 October 2019

DOI: 10.1111/ter.12430

PAPER

Terra Nova WILEY

Co-seismic deformation and post-glacial slip rate along the Magallanes-Fagnano fault, Tierra Del Fuego, Argentina

Sandrine Roy[1] | Riccardo Vassallo[1] | Joseph Martinod[1] | Matías C. Ghiglione[2] | Christian Sue[1,3] | Pascal Allemand[4]

[1]ISTerre, Univ. Grenoble Alpes, Université Savoie Mont Blanc, CNRS, IRD, IFSTTAR, Grenoble, France

[2]IDEAN-CONICET – Universidad de Buenos Aires, Buenos Aires, Argentina

[3]CNRS UMR6249, Université Bourgogne Franche-Comté, Besançon, France

[4]Laboratoire de Géologie, Université Claude Bernard Lyon 1, Villeurbanne, France

Correspondence
Sandrine Roy, Institute of Earth Sciences ISTerre, Université Savoie Mont Blanc, 73376 Le Bourget-du-Lac, Grenoble, France.
Email: s.roy.unistra@gmail.com

Funding information
Direction Générale de la Recherche Scientifique et du Développement Technologique, Grant/Award Number: PhD Scholarship Sandrine ROY; Argentinian-French ECOS-SUD, Grant/Award Number: A15U02

Abstract

Across the extreme south of Patagonia, the Magallanes-Fagnano Fault (MFF) accommodates the left-lateral relative motion between South America and Scotia plates. In this paper, we present an updated view of the geometry of the eastern portion of the MFF outcropping in Tierra del Fuego. We subdivide the MFF in eight segments on the basis of their deformation styles, using field mapping and interpretation of high-resolution imagery. We quantify coseismic ruptures of the strongest recorded 1949, M_w7.5 earthquake, and determine its eastern termination. We recognize several co-seismic offsets in man-made features showing a sinistral shift up to 6.5 m, greater than previously estimated. Using ^{10}Be cosmogenic nuclides depth profiles, we date a cumulated offset in post-glacial morphologies and estimate the long-term slip rate of the eastern MFF. We quantify a 6.4 ± 0.9 mm/a left-lateral fault slip rate, which overlaps geodetic velocity and suggests stable fault behaviour since Pleistocene.

1 | INTRODUCTION

The Magallanes-Fagnano Fault (MFF) accommodates the sinistral motion between the Scotia and South America plates along a 600 km fault system that crosses the Isla Grande de Tierra del Fuego from the western channel of the Magellan Strait to the Atlantic coast (Figure 1a). This active transform boundary continues eastward along the North Scotia Ridge towards South Georgia (Betka, Klepeis, & Mosher, 2016; Dalziel, Lawver, Norton, & Gahagan, 2013; Esteban, Tassone, Isola, Lodolo, & Menichetti, 2018; Klepeis, 1994). In Tierra del Fuego, GNSS data indicate that active deformations are localized on the MFF, and that present-day fault velocity ranges between ~5.9 ± 0.2 mm/a (Mendoza et al., 2015) and ~6.6 ± 1.3 mm/a (Smalley et al., 2003). The locking depth of the eastern MFF is estimated at about 11 ± 5 km (Mendoza et al., 2015).

In this work, we focus on the Eastern MFF between the Fagnano Lake and the Atlantic coast in Tierra del Fuego (Figure 1b). Two major seismic events occurred in 1879 and 1949. On the 1 February 1879, several European settlements reported an earthquake of intensity VII Modified Mercalli Scale (MMS) near Punta Arenas and VIII MMS in Tierra del Fuego (Cisternas & Vera, 2008), that was later estimated having magnitude 7–7.5 (Lomnitz, 1970). In 1949, two main earthquakes occurred on December 17 at 6:53 (GMT) (M_w7.75), and at 15:07 (GMT) (M_w7.5), followed by several aftershocks of unknown magnitude (Febrer, Plasencia, & Sabbione, 2000; Jaschek, Sabbione, & Sierra, 1982). We report in Figure 1b the position of 1949 epicentres according to different authors. Co-seismic surface ruptures (Figure 2a) were described at Fagnano and Udaeta Lakes shoreline and in the Estancia La Correntina (Costa et al., 2006; Lodolo et al., 2003; Pedrera et al., 2014). The maximum horizontal component associated with the 1949 ruptures was estimated up to 4 m (Costa et al., 2006).

Intertwined with the tectonic activity, the landscape of Tierra del Fuego has been shaped by the alternating advance and retreat of the Fuegian Patagonian ice-sheet (Coronato, Seppälä, Ponce, & Rabassa, 2009; Glasser & Ghiglione, 2009; Waldmann, 2008; Waldmann, Ariztegui, Anselmetti, Coronato, & Austin, 2010). A major glacial lobe

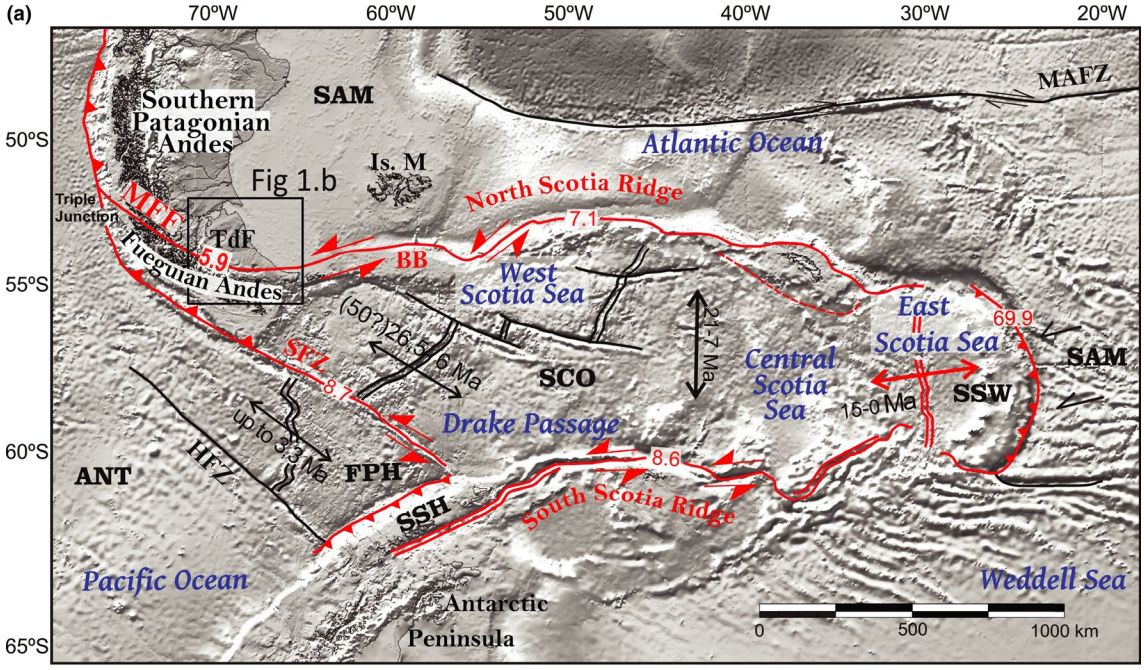
(a)
70°W
60°W
50°W
40°W
30°W
20°W
50°S
55°S
60°S
65°S
Southern Patagonian Andes
SAM
Is. M
Fig 1.b
Triple Junction
MFF
TdF
Fuegian Andes
5.9
BB
North Scotia Ridge
7.1
West Scotia Sea
(50-?)26-6 Ma
SFZ
8.1
SCO
21-7 Ma
Central Scotia Sea
East Scotia Sea
69.9
SAM
SSW
15-0 Ma
MAFZ
Atlantic Ocean
Drake Passage
up to 3-3 Ma
HFZ
ANT
FPH
SSH
8.6
South Scotia Ridge
Pacific Ocean
Antarctic Peninsula
Weddell Sea
0
500
1000 km

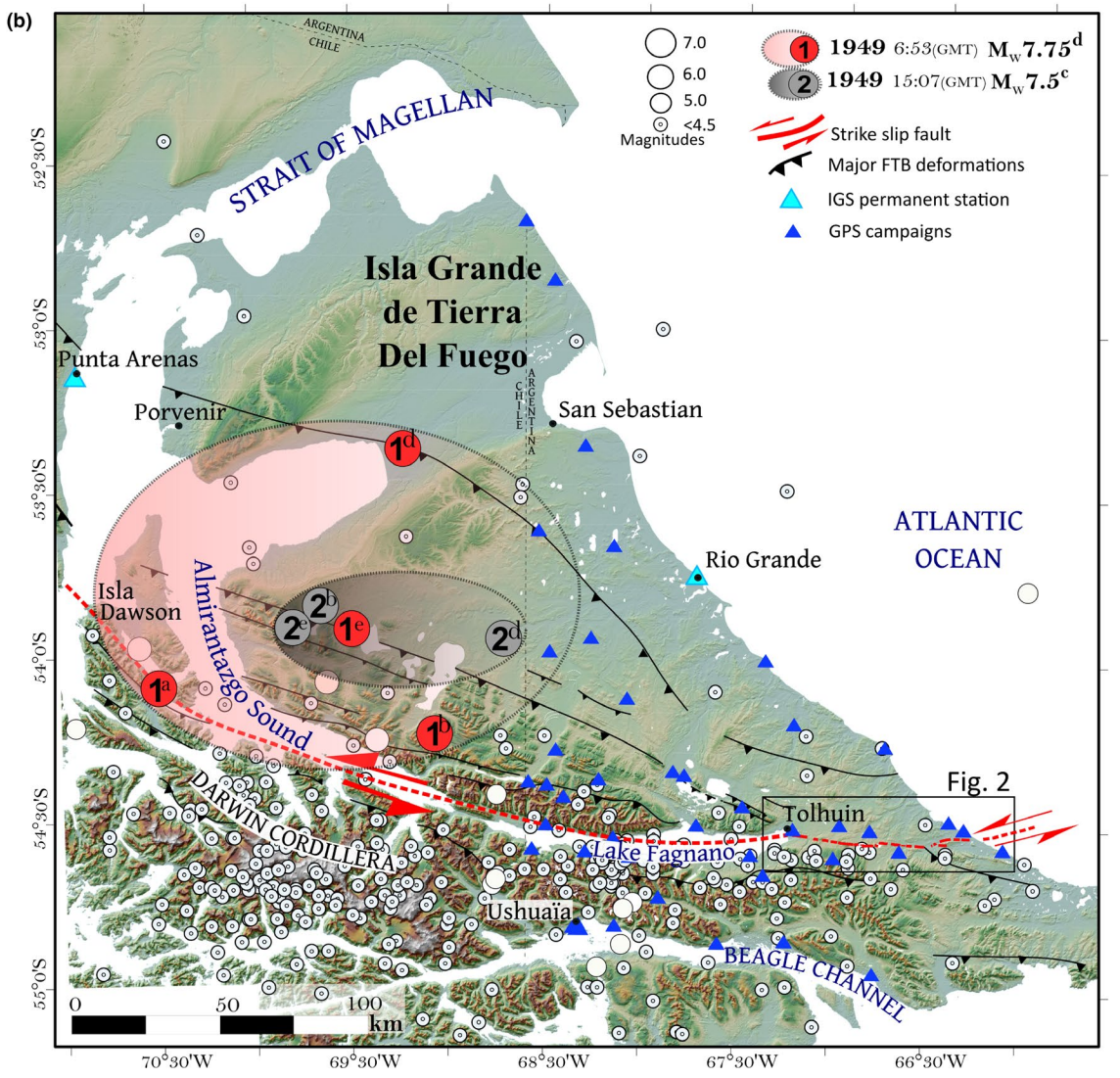
(b)
ARGENTINA
CHILE
7.0
6.0
5.0
<4.5
Magnitudes
1 1949 6:53(GMT) Mw7.75d
2 1949 15:07(GMT) Mw7.5c
Strike slip fault
Major FTB deformations
IGS permanent station
GPS campaigns
STRAIT OF MAGELLAN
Isla Grande de Tierra Del Fuego
Punta Arenas
Porvenir
San Sebastian
ATLANTIC OCEAN
Rio Grande
Isla Dawson
Almirantazgo Sound
DARWIN CORDILLERA
Tolhuin
Fig. 2
Lake Fagnano
Ushuaia
BEAGLE CHANNEL
0
50
100
km
52°30'S
53°0'S
53°30'S
54°0'S
54°30'S
55°0'S
70°30'W
69°30'W
68°30'W
67°30'W
66°30'W

FIGURE 1 (a) Tectonic setting of southernmost Andes with plate boundary velocities (mm/a) (from: Barker, 2001; Dalziel et al., 2013; Ghiglione et al., 2010; Thomas, Livermore, & Pollitz, 2003), superimposed on greyscale topography and bathymetry (Sandwell & Smith, 1997). Relative strike-slip motion of MFF from (Mendoza et al., 2015). Red lines are active structures; black lines are extinct tectonic features. ANT, Antarctic plate; BB, Burdwood Bank; FPH, Former Phoenix plate; HFZ, Hero Fracture Zone; Is. M, Islas Malvinas; MFF, Magallanes-Fagnano Fault; MAFZ, Malvinas-Agulhas Fracture Zone; SAM, South America plate; SCO, Scotia plate; SFZ, Shackleton Fracture Zone; SSH, South Shetland plate; SSW, South Sandwich plate, TdF, Isla Grande de Tierra del Fuego. (b) Faults and seismicity of Tierra del Fuego. The trace of the MFF is shown with a red dotted line, and the major fold-thrust belt (from Glasser & Ghiglione, 2009) are shown with black lines. We reported historical 1949 earthquakes epicentre locations proposed by (a) Castano (1977); (b) Jaschek et al. (1982); (c) Lomnitz (1970); (d) Pelayo and Wiens (1989); (e) U.S. Geological Survey (2017); Red and grey shaded ellipses refer to the most consistent region for epicentre location of the two main 1949 shocks. Catalogue of earthquakes are from (Buffoni, Sabbione, Connon, & Ormaechea, 2009; Febrer et al., 2000; Flores Véliz, 2017; Pelayo & Wiens, 1989). Locations of GPS sites measured in Mendoza et al. (2015) [Colour figure can be viewed at wileyonlinelibrary.com]

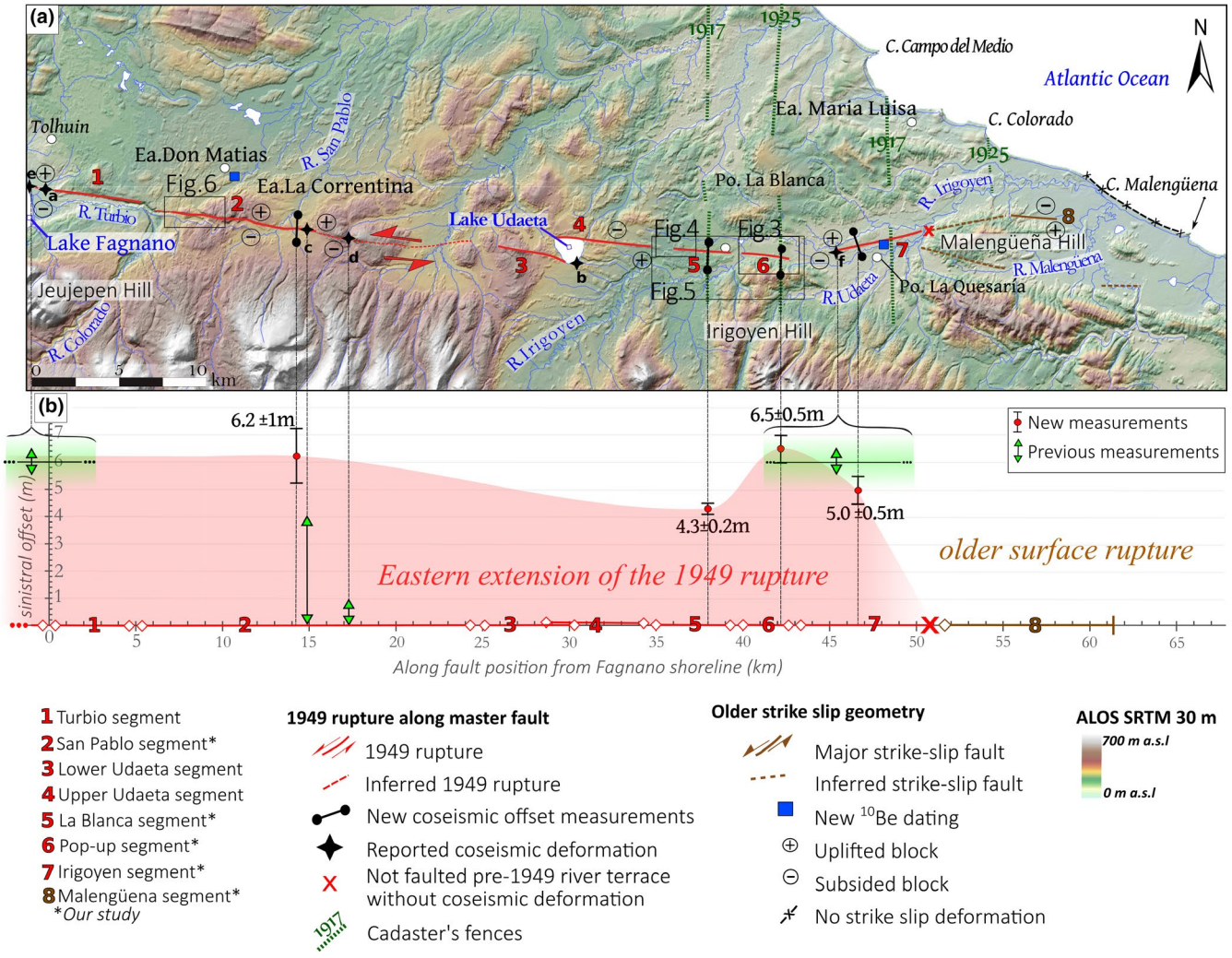

FIGURE 2 (a) Structural map of the eastern MFF. The 1949 surface ruptures are shown as red lines, and the segments with evidences of long-term slip are shown as brown lines. The red cross symbolizes the eastern termination of the 1949 surface rupture. Reported coseismic surface deformations: (a) sag pond and vertical scarp (~0.5 to 1 m) in Fagnano gravel bar (Lodolo et al., 2003); (b) liquefaction and truncated-tree line features (Onorato et al., 2016; Pedrera et al., 2014); (c) and (d), respectively, 'San Pablo' and 'Oliva' disrupted fences mentioned by (Costa et al., 2006). (e) and (f) show two previous reported offsets by eyewitnesses without exact locations (Costa et al., 2006). The relative uplifted blocks are shown with a circled plus sign. The base map is DEM SRTM ALOS Word 3D-30m (© JAXA). (b) 1949 sinistral horizontal offsets along the eastern MFF. Red dots and their associated error bars correspond to measurements from this study. Previous reported offset using green triangles and green shaded rectangles showing the range of possible locations. The 1949 surface rupture continues westward through the Fagnano lake [Colour figure can be viewed at wileyonlinelibrary.com]

flowed eastward from the Darwin Cordillera (Figure 1b) and carved a deep valley now partly occupied by the Fagnano Lake, while east of the lake, smaller tributary glaciers flowed northward above the fault, and eroded part of the pre-glacial strike-slip morphologies (Coronato, Meglioli, & Rabassa, 2004). Consequently, the reconstruction of the last deglaciation timing and the related deposit locations are crucial

to understand when and where post-glacial strike-slip faulting were recorded. In our work, we built high resolution digital elevation model from Pléiades images combined with extensive field work to study the remarkable imprint of the tectonic activity left in the glaciofluvial deposits and analyse the geometry and kinematics of the fault ruptures.

The Holocene activity of the MFF has been studied at some specific sites by Costa et al. (2006), Waldmann et al. (2011), Esteban et al. (2014), Onorato, Perucca, Coronato, Rabassa, and López (2016), Perucca, Alvarado, and Saez (2016). In this paper, we present a detailed description of the 65-km long onshore part of the fault located east of Fagnano Lake, including the previously unstudied 30 km-long segments located east of Udaeta lake. We describe the 1949 rupture, and reassess the horizontal offset and the coseismic rupture length with new observations of unprecedented described features. Finally, we describe the geomorphic cumulated offset to constrain the average MFF long-term slip rate since the Late-Pleistocene.

2 | EASTERN MFF GEOMETRY

East of Fagnano Lake, the MFF strike is N90°–95°, i.e. sub-parallel to the Palaeogene structures that conform the Fuegian thin-skinned fold and thrust belt (Ghiglione & Ramos, 2005; Klepeis & Austin, 1997). We subdivide the fault into eight segments with their singular geomorphic expressions. All segments are characterized by a main strike-slip kinematics, however, a moderate dip-slip component results in the relative uplift of either the southern or northern block (Figure 2). The deformation style varies along the 65 km length of the fault and exposes both localized and more distributed patterns. We observe on most of the segments Riedel faults (Figure 3a) with a minor vertical component. Orientations indicate R-shear synthetic fractures ranging N70-75° (Figure 3).

In other segments, the tectonic deformation is distributed off fault in a sheared zone. At the northern foothill of Sierra Irigoyen along segment 6, we identify a 3-km-long alignment of hectometric pop-up structures (Figure 4a). They consist in asymmetric 2–6 m-high rhomboidal hills, elongated in their ENE, WSW axis. The inner part exposes N80°-striking Riedel faults (Figure 4b,d). On pop-ups, trees trunks of 100 years old are progressively tilted towards the external border, evidencing that the elevation of these structures amplified during the last earthquake (Figure 4c,e). This particular expression of surface deformation, distributed on transpressive structures, is located in an active flood plain. The presence of unconsolidated sand material and water may favour this deformation style.

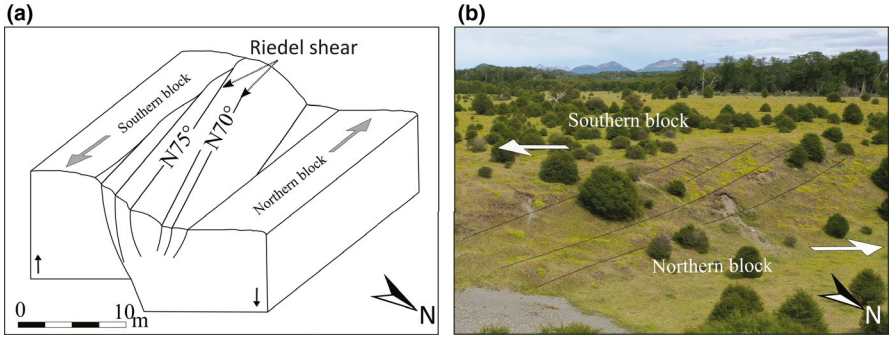

FIGURE 3 Deformation style of the segment 5 (a) Block diagram of Riedel faults with a long-term dip-slip component; (b) Field photography of the Riedel faults [Colour figure can be viewed at wileyonlinelibrary.com]

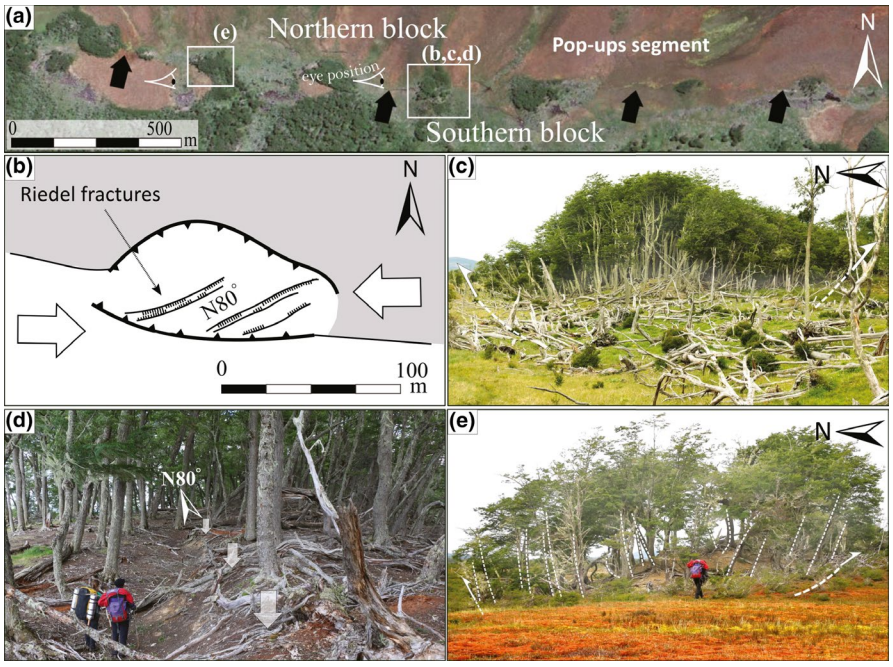

FIGURE 4 Geometry and style of the pop-up structures along segment 6 (a) General view of the pop-ups alignment (green forested patches); (b) detailed structural sketch of one pop-up showing Riedel faults; (c) pop-up structure with fan shaped tilted trees; (d) Riedel fault within a pop-up; (e) pop-up structure with tilted tree [Colour figure can be viewed at wileyonlinelibrary.com]

3 | THE 1949 CO-SEISMIC RUPTURE

Costa et al. (2006) interviewed several eyewitnesses of the 1949 earthquakes and concluded that the horizontal offset did not exceed 4 m. Some witnesses however reported lateral offsets as large as 6 m. Unfortunately, these observations are not supported by field measurements and their precise location is missing. A more exhaustive and accurate offsets estimation is therefore fundamental to improve earthquake scaling behaviour for this fault.

We observe many preserved markers of the co-seismic ruptures from the last earthquake sequence, some of them giving information on the 1949 sinistral offset. Two offsets have been measured (Figure 5) in sheep fences corresponding to the Argentinean land registers of the early 20th century (Casali & Manzi, 2017). These limits correspond to several tens of kilometres N–S straight wired connected fences which can easily be mapped from satellite images (Figure 5a). In segments 5 and 6, fence offsets evidence a 4 ± 0.2 m and a 6.5 ± 0.5 m sinistral shift, respectively (Figure 5b,c). However, it is not possible discriminating whether the offset originated from one or from the sum of the two successive shocks. Also, no evidence of creeping has been noticed since the new fences replaced the pre-1949 ones (Figure 5d).

Another offset is measured at the segment 7 (Figure 2), where N75° lineament have been previously noticed (Ghiglione, 2003). The fault is crossed by a stream flowing southward which undergoes a sharp sinistral offset of 5 m ± 0.5 m. Besides, in the segment 2 a 6.2 ± 1 m sinistral offset is also visible in the foundations of an abandoned broken bridge that spanned over the fault line. These field measurements evidence the horizontal component of the rupture on different segments and show that largest offsets are up to 6–6.5 m. This value is higher than previously measured (4 m) and is consistent with observations noticed by eyewitnesses of the 1949 event.

The easternmost offset measured is localized within the segment 7. Eastward, no geomorphic evidence of the rupture could be observed in pre-1949 river terraces, suggesting that the surface rupture did not propagate farther east (Figure 2b). Along the segment 8, the fault trace is visible in a continuous 5 m-high scarp. However, this scarp is much more degraded than in the western segments. These characteristics are consistent with the occurrence of older ruptures along this segment. We did not observe any strike-slip evidence between the Colorado and Malengüeña Capes.

Our observations show that 1949 co-seismic rupture zone ended at 50 km east of the Lake Fagnano shoreline. Westward of our study zone, the rupture continues across the Fagnano lake parallel to its EW elongate geometry. It could die out somewhere along the 100 km of the lake or continue further west in

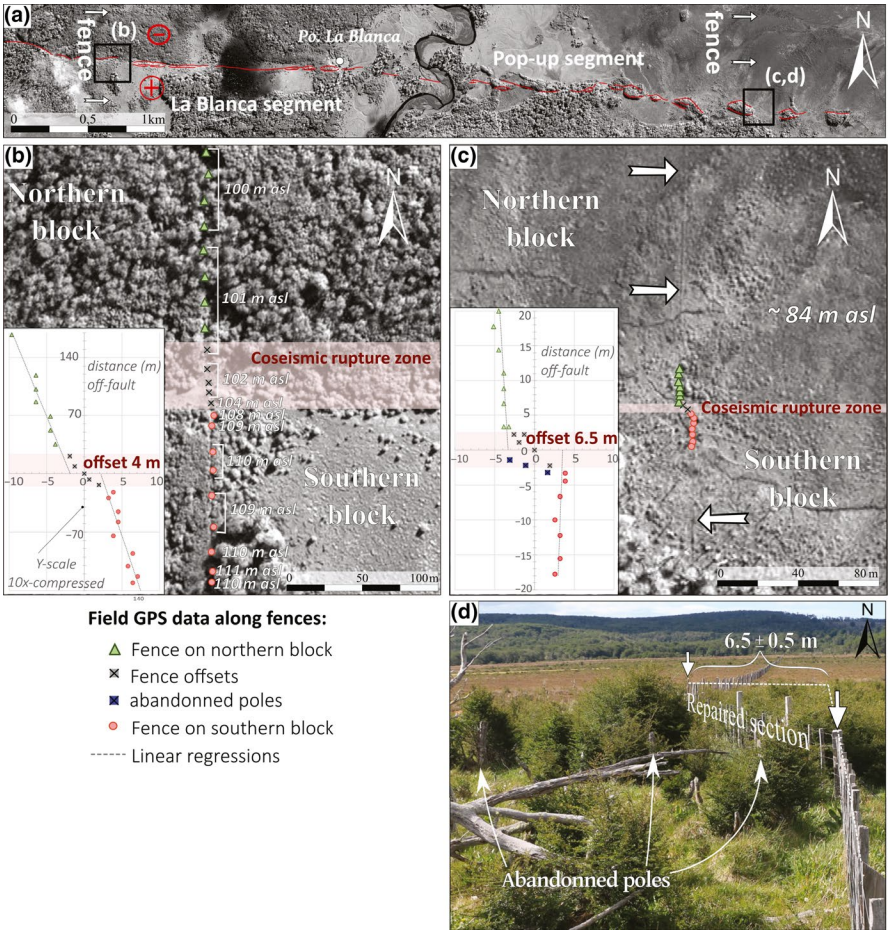

FIGURE 5 (a) Pléiade image above the fault segments 5 and 6 showing the location of offset fences. (b) and (c) GPS points along fences superimposed on Pléiade images, respectively, at segments 5 and 6. Note: on the figure (b) the NS scale of the lower graph has been compressed 10 times. White arrow in (c) highlight the trace of the fences away from the coseismic rupture zone. (d) Photography of measured sinistral offset along the segment 6, showing some of the disrupted fence abandoned poles [Colour figure can be viewed at wileyonlinelibrary.com]

the Magellan Strait. Nevertheless, the lack of observation on the western part of the MFF prevent to identify the 1949 surface ruptures termination.

4 | POST-GLACIAL SLIP RATE

Here, we use the changes in the hydrological network following the Fuegian glaciers retreat to assess the post-glacial long-term slip rate.

The segment 2 crosscuts four well-defined geomorphic markers within a 2 km-long zone (Figure 2a): a dead valley, its associated meander, one topographic depression and one ridge (Figure 6a). We use the respective edges of the geomorphic markers (Figure 6b) to assess the left-lateral offset using the back-slip restoration technique (e.g. Klinger et al., 2005; McGill & Sieh, 1991). The piercing points all match with the best correlation at 115 ± 5 m displacement (Figure 6c).

This restoration shows that these various markers are synchronous and probably related to a main landscape formation phase corresponding to the ice retreat. After restoration, the dead-valley recovers its characteristic shape before the abandonment. This valley was carved by meltwater streams following the retreat of tributary glaciers. Such glaciers have also been described further to the west in JeuJepen hill (Figure 2a; Coronato, Roig, & Mir, 2002). Glacial and Glaciofluvial erosion erased previous strike-slip offset. Such markers fix the beginning of the tectonic surface deformation record in this segment, providing a relative slip chronometer.

By dating the exposure of the youngest sediments of the fossil drainage system, we date the abandonment of the valley and the onset of the subsequent tectonic deformation record. Sampling took place respectively near the Estancia Don Matias and the Puesto La Quesaria (Figure 2a) with established procedures (Braucher, Brown, Bourlès, & Colin, 2003; Ritz et al., 2006). We sampled quartz cobbles for cosmic ray exposure dating using ^{10}Be along two vertical profiles. Surfaces are flat and underwent negligible erosion, thus we assume a zero denudation rate for age calculations. We use the least-square

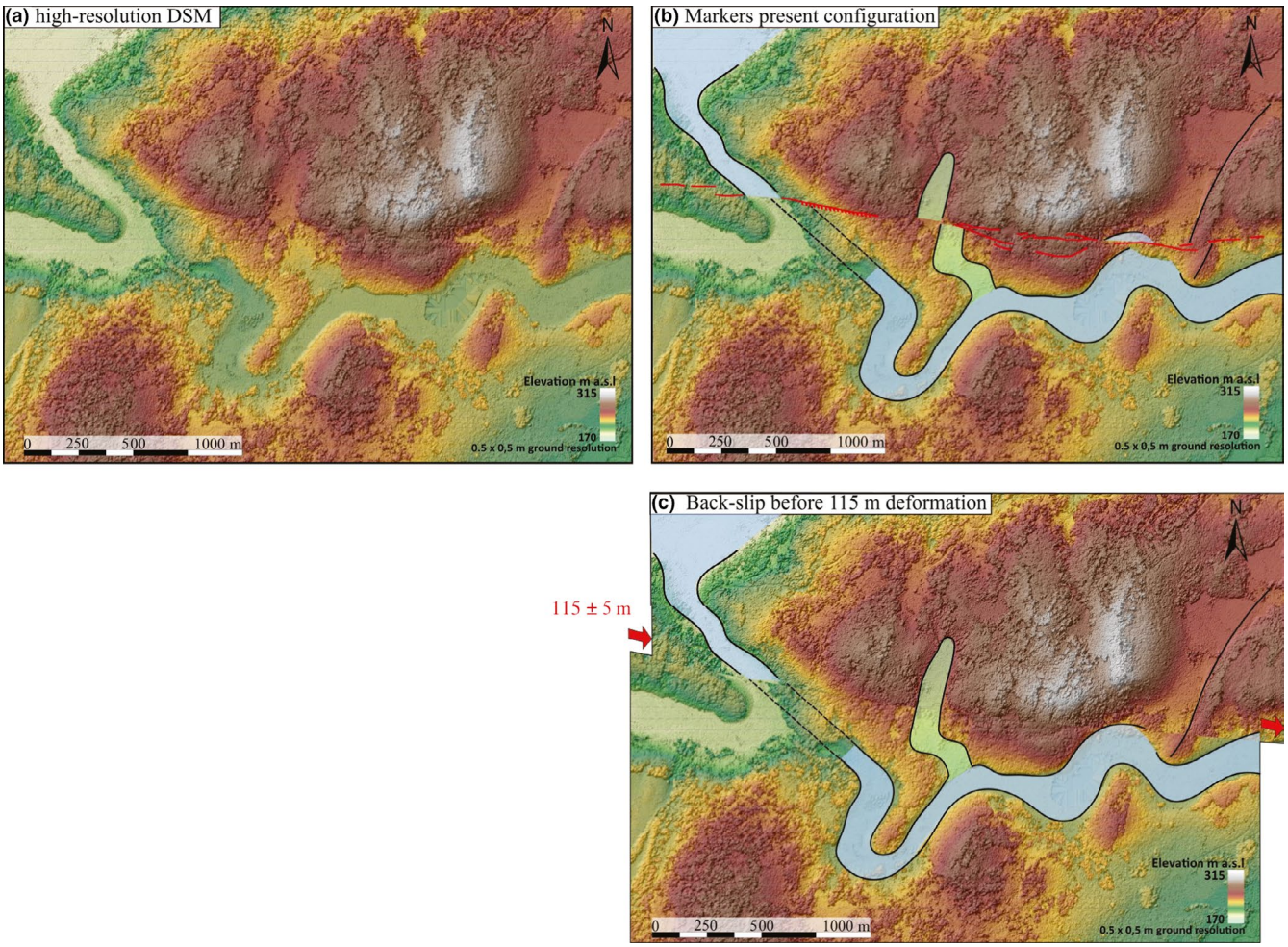

FIGURE 6 Back-slip deformation of post-glacial morphologies along segment 2. (a) High resolution DSM showing the dead valley drainage system, (b) markers superimposed on DSM with strike-slip (red lines), and offsets in geomorphic markers (black lines): abandoned valley with associated truncated meander (blue cover), hanging valley (green cover) and a hill's ridge (single black line). Lines are used as piercing point crossing the fault trace. We projected each flank of the abandoned valley on the fault plane to identify piercing points. (c) Back slip deformation of markers, the piercing points match for 115 ± 5 m cumulated offset [Colour figure can be viewed at wileyonlinelibrary.com]

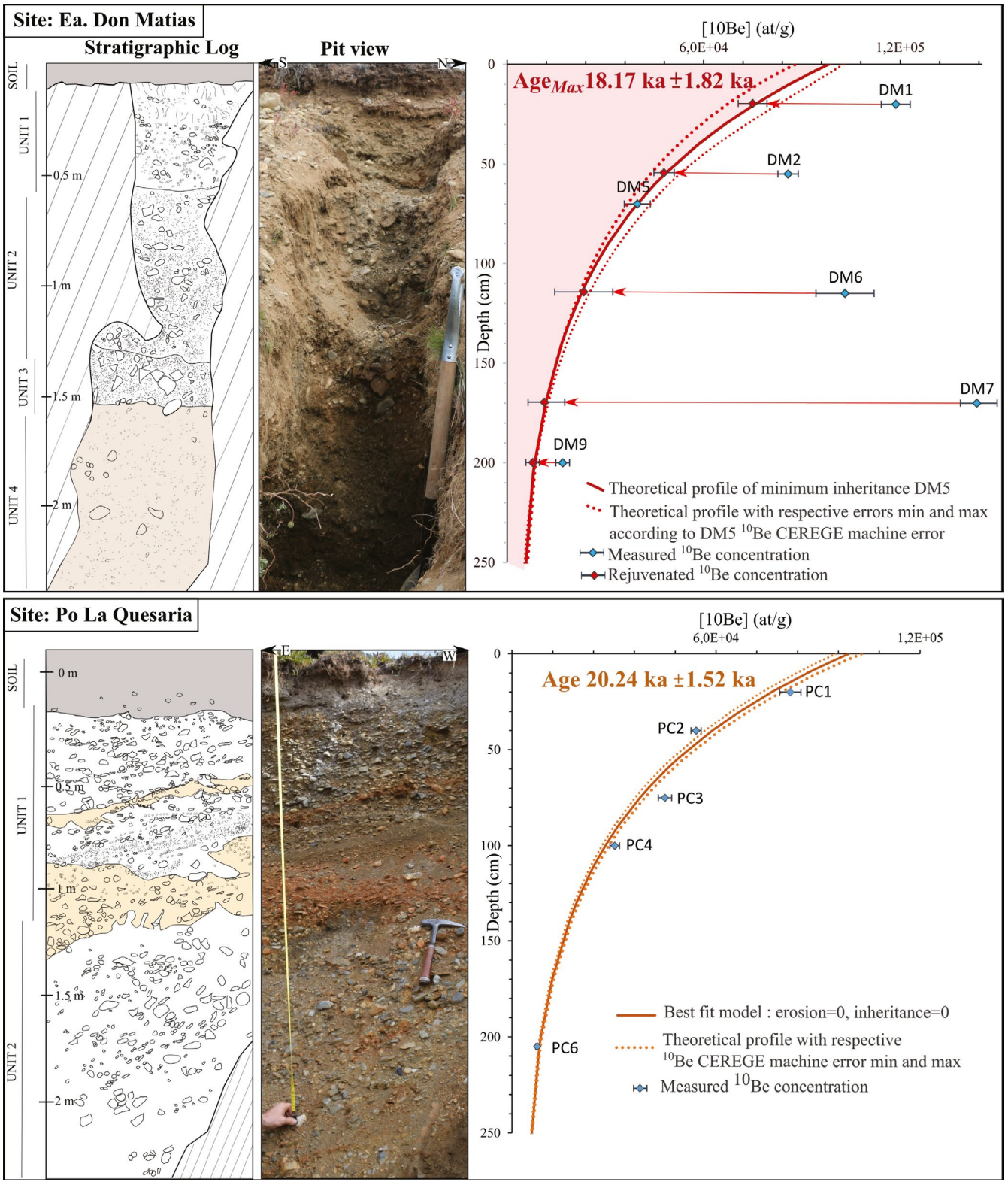

FIGURE 7 ^{10}Be depth profiles with respective stratigraphic log and pit view of site Estancia Don Matias and Puesto La Quesaria (see Figure 2 for location). ^{10}Be production rate has been calibrated for local latitudes and elevations (Stone, 2000), using the modified functions of (Lal, 1991), which stands in quartz production of 4.92 ± 0.43 at g^{-1} a^{-1} at sea level and high latitude. Calculations were performed using attenuation lengths of 150, 1,500 and 5,300 g/cm^2 with associated relative contributions of 97.85%, 1.50% and 0.65% (Braucher et al., 2003). We employ the currently accepted ^{10}Be half-life value of 1.387 ± 0.012 106 years (Chmeleff, Blanckenburg, Kossert, & Jakob, 2010; Korschinek et al., 2010; Nishiizumi et al., 2007). Measurements were completed at the accelerator mass spectrometry facility ASTER (Aix-en-Provence, France) after preparation at the ISTerre GeoThermoChronology platform (Grenoble, France) [Colour figure can be viewed at wileyonlinelibrary.com]

inversion to model theoretical curves on both profiles for ^{10}Be concentration measurements.

Estancia Don Matias' terrace stratigraphic log presents four faciès of well-sorted sandy gravel matrix with gradational contacts resulting from glaciofluvial depositions (Figure 7). The predominance of subangular and subrounded clasts in the two lower levels (unit 3 and 4) indicates a short glaciofluvial transport. The concentrations distribution does not decrease exponentially with depth, evidencing that sample may have two exposure sources: the common post-depositional cosmogenic nuclide production and their own pre-depositional production, which is responsible for an intrinsic ^{10}Be inheritance value. Based on these hypotheses, we apply the profile rejuvenation methodology (Le Dortz et al., 2012). We select the sample (DM5) with the minimum ^{10}Be concentration normalized by depth. It has the lowest inherited concentration among all the profile samples. Its apparent exposure age is, therefore, the closest to the true post-depositional age of the valley. The ^{10}Be concentration of sample DM5 yields a maximum age of valley abandonment at ~18 ± 2 ka. This age fixes the beginning of the tectonic deformation record. In the same area, age based on ^{14}C of basal peat bog grown on top of moraine deposits confirm that ice retreat in this region started before ~14 ka (Coronato et al., 2009).

At Puesto La Quesaria, we sampled the highest preserved alluvial terrace, whose formation is supposed to be synchronous of regional glacial retreat. The profile exposes pebble to gravel clasts in a sandy matrix characteristic of meltwater channel environment (Figure 7). Here, the distribution of ^{10}Be concentrations decreases exponentially with depth following the theoretical curve of ^{10}Be production (Brown et al., 1991; Dunai, 2010), suggesting that inherited cosmogenic concentrations are negligible compared to post-depositional concentrations. These concentrations yield a terrace exposure age of 20.2 ± 1.5 ka, overlapping the maximum age obtained near the Estancia Don Matias.

These ages characterize the main recession phase during which the tributaries glaciers retreated above the Southern Hills (Coronato et al., 2009; Rabassa, Coronato, & Martínez, 2011; Waldmann et al., 2010). The abandonment of the glaciofluvial valleys resulting from ice retreat fossilized the associated drainage system allowing the preservation of fault activity in the landscape since 18–20 ka. The cumulated offset observed in the valley near by the Estancia Don Matias since this period yields a geomorphic slip-rate of 6.4 ± 0.9 mm/a.

5 | DISCUSSION AND CONCLUSIONS

We explore the main post-glacial deformations recorded along the eastern sector of the MFF from Lake Fagnano to the Atlantic coast and integrated previously documented geometries. Newly described strike-slip structures, pop-ups, and Riedel fractures are mapped with the relative vertical motion of blocks. The analysis of high-resolution topographic models and satellite images does not show any significant deformation on secondary structures, confirming that strike-slip motion concentrates along the master fault as already suggested by GPS data inversion (Mendoza et al., 2011).

We chart the 1949 surface primary ruptures and measured related sinistral slips. We document horizontal offsets up to 6.5 ± 0.5 m. Surface rupture can be followed along 50 km from the Fagnano Lake shoreline to the tip of the segment 7. According to the main shocks magnitudes the 1949 surface rupture probably continued beneath Fagnano Lake, but the lack of direct access to the western part of the MFF prevent to identify the 1949 western surface ruptures termination.

Back-slip restoration of offset glaciofluvial markers combined with ^{10}Be dating allow the first quantification of the geomorphic slip rate for this fault. The offset started to accumulate when the local glacial catchment source vanished and associated drainage system was abandoned ~18 ± 2 ka ago. Our results yield a left-lateral Late Pleistocene slip rate of 6.4 ± 0.9 mm/a over this period. This value overlaps the present-day velocity estimated using geodetic data. The unchanged fault slip rate over the different time-scale suggests a stable fault behaviour since glaciers retreat.

Previous indirect attempts of major MFF earthquake recurrence estimations are divergent and possibly biased by the method used. The shorter proposed recurrence interval is about 350–850 years (Waldmann et al., 2011) while the longer is 3,000–4,500 years (Costa et al., 2006). The former study uses as a proxy the mass-wasting events in Fagnano Lake, which may integrate events triggered on other structures, while the latter is based on a single palaeoseismological trench, in which sedimentary and tectonic record are not complete and some events may not be registered. Considering the 1949 co-seismic offsets in the area around the long-term slip-rate measurement, we obtained an average offset of 6 ± 0.5 m. With a geomorphic slip rate of 6.4 ± 0.9 mm/a, and based on the average co-seismic offset of 1949, we propose a frequency of large earthquakes event about 1,000 ± 215 years.

ACKNOWLEDGEMENTS

This research is part of a bilateral scientific cooperation project between Argentinian Mincyt—Universidad de Buenos Aires, and the University Savoie Mont-Blanc (ISTerre) and the Besancon University, funded by the Argentinian-French ECOS-SUD under grant project A15U02. We acknowledge the French CNRS-INSU (project PICS and SYSTER). We address special thanks to J. Carcaillet (ISTerre GeoThermoChronology platform) for his guidance in cosmogenic dating and warmly thank F. Massot and O. Romeyer for their technical support. We are also deeply grateful to M. P. Escayola (UNTDF Universidad Tierra Del Fuego), M. Bauducco and C. Maure for their direct and efficient support in Tierra del Fuego. The authors thank J.L. Paños, E.S. Ampuero, K.A.Vargas Saldivia, and P.J. López, for kindly authorizing us to work on their lands. The manuscript was greatly improved due to careful reviews by F. Visini, P. Burrato and Associate Editor C. Chiarabba.

DATA AVAILABILITY STATEMENT

The data that support the findings of this study are available on request from the corresponding author.

ORCID

Sandrine Roy https://orcid.org/0000-0003-3541-7765
Riccardo Vassallo https://orcid.org/0000-0003-2785-8835
Matías C. Ghiglione https://orcid.org/0000-0002-0243-3251
Christian Sue https://orcid.org/0000-0002-2472-5001
Pascal Allemand https://orcid.org/0000-0003-1269-6298

REFERENCES

Barker, P. F. (2001). Scotia sea regional tectonic evolution: Implications for mantle flow and palaeocirculation. *Earth-Science Reviews*, *55*, 1–39. https://doi.org/10.1016/S0012-8252(01)00055-1

Betka, P., Klepeis, K., & Mosher, S. (2016). Fault kinematics of the Magallanes-Fagnano fault system, southern Chile: An example of diffuse strain and sinistral transtension along a continental transform margin. *Journal of Structural Geology*, *85*, 130–153. https://doi.org/10.1016/j.jsg.2016.02.001

Braucher, R., Brown, E. T., Bourlès, D. L., & Colin, F. (2003). In situ produced ^{10}Be measurements at great depths: Implications for production rates by fast muons. *Earth and Planetary Science Letters*, *211*, 251–258. https://doi.org/10.1016/S0012-821X(03)00205-X

Brown, E. T., Edmond, J. M., Raisbeck, G. M., Yiou, F., Kurz, M. D., & Brook, E. J. (1991). Examination of surface exposure ages of Antarctic moraines using in situ produced ^{10}Be and ^{26}Al. *Geochimica et Cosmochimica Acta*, *55*, 2269–2283. https://doi.org/10.1016/0016-7037(91)90103-C

Buffoni, C., Sabbione, N. C., Connon, G., & Ormaechea, J. L. (2009). Localización De Hipocentros Y Determinación De Su Magnitud En Tierra Del Fuego Y Zonas Aledañas. *GeoActa*, *34*, 75–86.

Casali, R., & Manzi, L. M. (2017). Etnicidades capitalistas: El rol de la Estancia San Pablo en el entramado de resistencia selk'nam. Tierra del Fuego, 1904–1930. *Magallania (Punta Arenas)*, *45*, 109–133. https://doi.org/10.4067/S0718-22442017000200109

Castano, J. C. (1977). Zonificación sísmica de la República Argentina. *Publicación Técnica*, *5*, 40.

Chmeleff, J., von Blanckenburg, F., Kossert, K., & Jakob, D. (2010). Determination of the ^{10}Be half-life by multicollector ICP-MS and liquid scintillation counting. *Nuclear Instruments and Methods in Physics Research Section B: Beam Interactions with Materials and Atoms*, *268*, 192–199. https://doi.org/10.1016/j.nimb.2009.09.012

Cisternas, A., & Vera, E. (2008). Sismos históricos y recientes en Magallanes. *Magallania (Punta Arenas)*, *36*, 43–51. https://doi.org/10.4067/S0718-22442008000100004

Coronato, A., Meglioli, A., & Rabassa, J. (2004). Glaciations in the Magellan Straits and Tierra del Fuego, southernmost South America. In J. Ehlers, & P. L. Gibbard (Eds.), *Developments in quaternary sciences, Quaternary glaciations extent and chronology. PART III: South America, Asia, Africa, Australia and Antarctica*. vol. 2. (pp. 45–48). Amsterdam, the Netherlands: Elsevier.

Coronato, A., Roig, C., & Mir, X. (2002). Geoformas glaciarias de la región oriental del Lago Fagnano, Tierra del Fuego, Argentina. In Actas XV Congreso Geológico Argentino. El Calafate, Argentina (23-26 de abril, 2002). CD-Rom. Artículo.

Coronato, A., Seppälä, M., Ponce, J. F., & Rabassa, J. (2009). Glacial geomorphology of the Pleistocene lake Fagnano ice lobe, Tierra Del Fuego, Southern South America. *Geomorphology*, *112*, 67–81. https://doi.org/10.1016/j.geomorph.2009.05.005

Costa, C. H., Smalley, R., Velasco, M. S., Schwart, D. P., Ellis, M., & Ahumada, E. A. (2006). Paleoseismic observations of an onshore transform boundary: The Magallanes-Fagnano fault, Tierra Del Fuego, Argentina. *Revista de la Asociación Geológica Argentina*, *61*(4), 647–657.

Dalziel, I. W., Lawver, L. A., Norton, I. O., & Gahagan, L. M. (2013). The Scotia arc: Genesis, evolution, global significance. *Annual Review of Earth and Planetary Sciences*, *41*, 767–793. https://doi.org/10.1146/annurev-earth-050212-124155

Dunai, T. J. (2010). *Cosmogenic Nuclides: Principles, concepts and applications in the Earth surface sciences*. Cambridge, UK: Cambridge University Press. https://doi.org/10.1017/CBO9780511804519

Esteban, F. D., Tassone, A., Isola, J. I., Lodolo, E., & Menichetti, M. (2018). Geometry and structure of the pull-apart basins developed along the western South American-Scotia plate boundary (SW Atlantic Ocean). *Journal of South American Earth Sciences*, *83*, 96–116. https://doi.org/10.1016/j.jsames.2018.02.005

Esteban, F. D., Tassone, A., Lodolo, E., Menichetti, M., Lippai, H., Waldmann, N., … Vilas, J. F. (2014). Basement Geometry and Sediment Thickness of Lago Fagnano (Tierra Del Fuego). *Andean Geology*, *41*, 293–313.

Febrer, J. M., Plasencia, M. P., & Sabbione, N. C. (2000). Local and regional seismicity from Ushuaia broadband station observations (Tierra del Fuego). *Terra Antartica*, *8*, 35–40.

Flores Véliz, M. C. (2017). Estudio de la sismicidad en la región de Magallanes. Facultad de Ciencias Fisicas y Matematicas, Universidad de Chile; Centro Sismológico National Universidad de Chile Informe de Práctica FCFM y CSN, 30 p.

Ghiglione, M. C. (2003). Estructura y evolución tectónica del Cretácico-Terciario de la costa Atlántica de Tierra del Fuego: *Estructura y Evolución Tectónica del Cretácico-Terciario de la costa atlántica de Tierra del Fuego*(PhD thesis) Ciudad De Buenos Aires (150 pp.).

Ghiglione, M. C., Quinteros, J., Yagupsky, D., Bonillo-Martínez, P., Hlebszevtich, J., Ramos, V. A., … Zapata, Y. T. (2010). Structure and tectonic history of the foreland basins of southernmost South America. *Journal of South American Earth Sciences*, *29*, 262–277. https://doi.org/10.1016/j.jsames.2009.07.006

Ghiglione, M. C., & Ramos, V. A. (2005). Progression of deformation and sedimentation in the southernmost Andes. *Tectonophysics*, *405*, 25–46. https://doi.org/10.1016/j.tecto.2005.05.004

Glasser, N. F., & Ghiglione, M. C. (2009). Structural, tectonic and glaciological controls on the evolution of fjord landscapes. *Geomorphology*, *105*, 291–302. https://doi.org/10.1016/j.geomorph.2008.10.007

Jaschek, E. U., Sabbione, N. C., & Sierra, P. J. (1982). Reubicación de sismos localizados en territorio Argentino, 1920–1963. Observatorio Astronomico de la Universidad nacional de la Plata.

Klepeis, K. A. (1994). The Magallanes and Deseado fault zones: Major segments of the South American-Scotia transform plate boundary in southernmost South America, Tierra Del Fuego. *Journal of Geophysical Research: Solid Earth*, *99*, 22001–22014. https://doi.org/10.1029/94JB01749

Klepeis, K. A., & Austin, J. A. (1997). Contrasting styles of superposed deformation in the southernmost Andes. *Tectonics*, *16*, 755–776. https://doi.org/10.1029/97TC01611

Klinger, Y., Xu, X., Tapponnier, P., Van der Woerd, J., Lasserre, C., & King, G. (2005). High-resolution satellite imagery mapping of the surface rupture and slip distribution of the M w~ 7.8, 14 November 2001 Kokoxili earthquake, Kunlun Fault, Northern Tibet, China. *Bulletin of the Seismological Society of America*, *95*, 1970–1987. https://doi.org/10.1785/0120040233

Korschinek, G., Bergmaier, A., Faestermann, T., Gerstmann, U. C., Knie, K., Rugel, G., … Remmert, A. (2010). A new value for the half-life of ^{10}Be by heavy-ion elastic recoil detection and liquid scintillation counting. *Nuclear Instruments and Methods in Physics Research Section B: Beam Interactions with Materials and Atoms*, *268*, 187–191. https://doi.org/10.1016/j.nimb.2009.09.020

Lal, D. (1991). Cosmic ray labeling of erosion surfaces: In situ nuclide production rates and erosion models. *Earth and Planetary Science Letters*, *104*, 424–439. https://doi.org/10.1016/0012-821X(91)90220-C

Le Dortz, K., Meyer, B., Sébrier, M., Braucher, R., Bourlès, D., Benedetti, L., … Foroutan, M. (2012). Interpreting scattered in-situ produced

cosmogenic nuclide depth-profile data. *Quaternary Geochronology*, *11*, 98–115. https://doi.org/10.1016/j.quageo.2012.02.020

Lodolo, E., Menichetti, M., Bartole, R., Ben-Avraham, Z., Tassone, A., & Lippai, H. (2003). Magallanes-Fagnano continental transform fault (Tierra del Fuego, southernmost South America). *Tectonics*, *22*, 15–26. https://doi.org/10.1029/2003TC001500

Lomnitz, C. (1970). Major earthquakes and tsunamis in Chile during the period 1535 to 1955. *Geologische Rundschau*, *59*, 938–960. doi:https://doi.org/10.1007/BF02042278.

McGill, S. F., & Sieh, K. (1991). Surficial offsets on the central and eastern Garlock fault associated with prehistoric earthquakes. *Journal of Geophysical Research: Solid Earth*, *96*, 21597–21621. 0148-0227/91/91JB-02030505.00

Mendoza, L., Perdomo, R., Hormaechea, J. L., Cogliano, D. D., Fritsche, M., Richter, A., & Dietrich, R. (2011). Present-day crustal deformation along the Magallanes-Fagnano Fault System in Tierra del Fuego from repeated GPS observations. *Geophysical Journal International*, *184*, 1009–1022. https://doi.org/10.1111/j.1365-246X.2010.04912.x

Mendoza, L., Richter, A., Fritsche, M., Hormaechea, J. L., Perdomo, R., & Dietrich, R. (2015). Block modeling of crustal deformation in Tierra del Fuego from GNSS velocities. *Tectonophysics*, *651–652*, 58–65. https://doi.org/10.1016/j.tecto.2015.03.013

Nishiizumi, K., Imamura, M., Caffee, M. W., Southon, J. R., Finkel, R. C., & McAninch, J. (2007). Absolute calibration of 10Be AMS standards. *Nuclear Instruments and Methods in Physics Research Section B: Beam Interactions with Materials and Atoms*, *258*, 403–413. https://doi.org/10.1016/j.nimb.2007.01.297

Onorato, M. R., Perucca, L., Coronato, A., Rabassa, J., & López, R. (2016). Seismically-induced soft-sediment deformation structures associated with the Magallanes-Fagnano Fault System (Isla Grande de Tierra del Fuego, Argentina). *Sedimentary Geology*, *344*, 135–144. https://doi.org/10.1016/j.sedgeo.2016.04.010

Pedrera, A., Galindo-Zaldívar, J., Ruiz-Constán, A., Bohoyo, F., Torres-Carbonell, P., Ruano, P., … González-Castillo, L. (2014). The last major earthquakes along the Magallanes-Fagnano fault system recorded by disturbed trees (Tierra del Fuego, South America). *Terra Nova*, *26*, 448–453. https://doi.org/10.1111/ter.12119

Pelayo, A. M., & Wiens, D. A. (1989). Seismotectonics and relative plate motions in the Scotia Sea region. *Journal of Geophysical Research: Solid Earth*, *94*, 7293–7320. 0148-0227/89/88JB-04217505.00

Perucca, L., Alvarado, P., & Saez, M. (2016). Neotectonics and seismicity in southern Patagonia. *Geological Journal*, *51*, 545–559. https://doi.org/10.1002/gj.2649

Rabassa, J., Coronato, A., & Martínez, O. (2011). Late Cenozoic glaciations in Patagonia and Tierra del Fuego: An updated review. *Biological Journal of the Linnean Society*, *103*, 316–335. https://doi.org/10.1111/j.1095-8312.2011.01681.x

Ritz, J.-F., Vassallo, R., Braucher, R., Brown, E. T., Carretier, S., & Bourlès, D. L. (2006). Using in situ-produced ^{10}Be to quantify active tectonics in the Gurvan Bogd mountain range (Gobi-Altay, Mongolia). *Special Papers-Geological Society of America*, *415*, 87–110. https://doi.org/10.1130/2006.2415(06)

Sandwell, D. T., & Smith, W. H. (1997). Marine gravity anomaly from Geosat and ERS 1 satellite altimetry. *Journal of Geophysical Research: Solid Earth*, *102*, 10039–10054. 0148-0227/97/96JB-03223$09.00

Smalley, R., Kendrick, E., Bevis, M. G., Dalziel, I. W. D., Taylor, F., Lauría, E., … Piana, E. (2003). Geodetic determination of relative plate motion and crustal deformation across the Scotia-South America plate boundary in eastern Tierra del Fuego. *Geochemistry, Geophysics, Geosystems*, *4*, 1070. doi:https://doi.org/10.1029/2002GC000446.

Stone, J. O. (2000). Air pressure and cosmogenic isotope production. *Journal of Geophysical Research: Solid Earth*, *105*, 23753–23759. https://doi.org/10.1029/2000JB900181

Thomas, C., Livermore, R., & Pollitz, F. (2003). Motion of the Scotia Sea plates. *Geophysical Journal International*, *155*, 789–804. https://doi.org/10.1111/j.1365-246X.2003.02069.x

U.S. Geological Survey (2017). Earthquake facts and statistics. National Earthquake Information Center, PDE.

Waldmann, N. (2008). Late Quaternary environmental changes in Lago Fagnano, Tierra del Fuego (54 S): reconstructing sedimentary processes, natural hazards and paleoclimate [Sc 4040]. Faculte Des Sciences, Département de géologie et de paléontologie, University of Geneve, 154 p.

Waldmann, N., Anselmetti, F. S., Ariztegui, D., Austin, J. A., Pirouz, M., Moy, C. M. and Dunbar, R. (2011). Holocene mass-wasting events in Lago Fagnano, Tierra del Fuego (54°S): implications for paleoseismicity of the Magallanes-Fagnano transform fault. *Basin Research*, *23*, 171–190. doi:https://doi.org/10.1111/j.1365-2117.2010.00489.x.

Waldmann, N., Ariztegui, D., Anselmetti, F. S., Coronato, A., & Austin, J. A. Jr (2010). Geophysical evidence of multiple glacier advances in Lago Fagnano (54 S), southernmost Patagonia. *Quaternary Science Reviews*, *29*, 1188–1200. https://doi.org/10.1016/j.quascirev.2010.01.016

How to cite this article: Roy S, Vassallo R, Martinod J, Ghiglione MC, Sue C, Allemand P. Co-seismic deformation and post-glacial slip rate along the Magallanes-Fagnano fault, Tierra Del Fuego, Argentina. *Terra Nova*. 2020;32:1–10. https://doi.org/10.1111/ter.12430